Video Article

In Vivo Dynamics of Retinal Microglial Activation During Neurodegeneration: Confocal Ophthalmoscopic Imaging and Cell Morphometry in Mouse Glaucoma

Alejandra Bosco[1], Cesar O. Romero[1], Balamurali K. Ambati[2], Monica L. Vetter[1]

[1]Department of Neurobiology & Anatomy, University of Utah

[2]Department of Ophthalmology & Visual Sciences, University of Utah

Correspondence to: Alejandra Bosco at alebosco@neuro.utah.edu

URL: https://www.jove.com/video/52731
DOI: doi:10.3791/52731

Keywords: Medicine, Issue 99, Neuroscience, microglia, neurodegeneration, glaucoma, retina, optic nerve head, confocal scanning laser ophthalmoscopy, live image analysis, segmentation by thresholding, cell morphometry CX3CR1, DBA/2J

Date Published: 5/11/2015

Citation: Bosco, A., Romero, C.O., Ambati, B.K., Vetter, M.L. *In Vivo* Dynamics of Retinal Microglial Activation During Neurodegeneration: Confocal Ophthalmoscopic Imaging and Cell Morphometry in Mouse Glaucoma. *J. Vis. Exp.* (99), e52731, doi:10.3791/52731 (2015).

Abstract

Microglia, which are CNS-resident neuroimmune cells, transform their morphology and size in response to CNS damage, switching to an activated state with distinct functions and gene expression profiles. The roles of microglial activation in health, injury and disease remain incompletely understood due to their dynamic and complex regulation in response to changes in their microenvironment. Thus, it is critical to non-invasively monitor and analyze changes in microglial activation over time in the intact organism. In vivo studies of microglial activation have been delayed by technical limitations to tracking microglial behavior without altering the CNS environment. This has been particularly challenging during chronic neurodegeneration, where long-term changes must be tracked. The retina, a CNS organ amenable to non-invasive live imaging, offers a powerful system to visualize and characterize the dynamics of microglia activation during chronic disorders.

This protocol outlines methods for long-term, *in vivo* imaging of retinal microglia, using confocal ophthalmoscopy (cSLO) and CX3CR1$^{GFP/+}$ reporter mice, to visualize microglia with cellular resolution. Also, we describe methods to quantify monthly changes in cell activation and density in large cell subsets (200-300 cells per retina). We confirm the use of somal area as a useful metric for live tracking of microglial activation in the retina by applying automated threshold-based morphometric analysis of *in vivo* images. We use these live image acquisition and analyses strategies to monitor the dynamic changes in microglial activation and microgliosis during early stages of retinal neurodegeneration in a mouse model of chronic glaucoma. This approach should be useful to investigate the contributions of microglia to neuronal and axonal decline in chronic CNS disorders that affect the retina and optic nerve.

Video Link

The video component of this article can be found at https://www.jove.com/video/52731/

Introduction

Microglia are neuroimmune cells that exclusively reside in the central nervous system (CNS) since early embryonic development and throughout adulthood. Equipped with a complex repertoire of receptors, microglial activity and regional heterogeneity are regulated by their bidirectional interplay with neighboring neurons, glia, blood-brain barrier and infiltrating neuroinflammatory cells[1,2]. Basal microglial functions contribute to physiological maintenance and repair, as they sample their territory for perturbations in homeostasis[3,4]. During CNS injury or disease, microglia are the first responders to neuronal signals that then trigger their transition to a reactive phenotype, termed “activated microglia[2,5-7]. Microglia activation involves an intricate cycle of gene and protein expression, which are coupled to cell soma and process resizing and remodeling[6-9]. Microglia activation, as well as cell redistribution and clustering, can be accompanied the local overall increase in the number of cells (termed microgliosis). This can result from cell proliferation and self-renewal, with or without recruitment of blood-derived monocytes[3,4,7,10-14]. In a broad range of age-dependent, chronic CNS diseases, sustained microgliosis and microglia activation parallel disease progression[15-19]. How microglia impact neurodegeneration remains unclear, mainly because they play both neuroprotective and deleterious roles that may have diverse contributions to disease onset and progression. Live imaging studies aimed at understanding chronic CNS disease have monitored microglial behavior in the damaged CNS of animal models and humans, and demonstrated that microglial alterations are detectable beginning at early disease stages[15-17,19,20]. Thus, it is critical to develop approaches to detect and monitor microglial activation *in vivo*.

Non-invasive detection of regional changes in brain microglia activation was established as an important *in vivo* indicator of neurodegenerative disease progression, using molecular imaging or bioluminescence and positron emission tomography or magnetic resonance imaging[18,21,22]. These highly quantitative and non-invasive molecular and nuclear imaging methods detect gliosis with regional resolution. Alternatively, two-photon confocal imaging in CX3CR1$^{GFP/+}$ mice has allowed the observation of brain microglia with cellular resolution[3,4,9,20,23-28]. However, this approach limits long-term and repeated observation of chronic microglial alterations, given the potential risk of disturbing their behavior by even minimally invasive brain imaging procedures[29]. Alternatively, the retina offers optimal conditions for direct, *in vivo* visualization and repeated

monitoring of microglia in their intact CNS niche throughout aging, following acute injury, and potentially during chronic neurodegenerative diseases. Thus, recent studies have proved the feasibility of high-resolution imaging of retinal microglia expressing GFP by adapting the confocal scanning laser ophthalmoscopy (cSLO) to image live CX3CR1$^{GFP/+}$ mice. This has been used to track weekly changes in GFP+ cell numbers in individual mice for up to 10 weeks following acutely induced injury or ocular hypertension[30-36].

We have extended this approach to perform long-term imaging over several months, and quantitatively track changes in microglia activation based on soma size using morphometric analysis. Somal size was defined as a useful metric of microglia activation in live imaging studies using two-photon confocal microscopy in cortical slices to perform *in vivo* imaging of CX3CR1-GFP+ microglia[9]. These and other studies also demonstrated the correlation between somal size and levels of Iba1 protein expression, which also increases with activation[9,37]. Thus, activated microglia can be identified in live mice, and their numbers and distribution monitored over time during CNS health and disease.

This protocol describes methods for cSLO live image acquisition and analysis to monitor microglial cell numbers, distribution and morphological activation during retinal ganglion cell (RGC) degeneration (**Figure 1**). Thus, this study uses: 1) a mouse model of inherited glaucoma (DBA/2J) that undergoes age-dependent optic nerve and retinal neurodegeneration and shows remarkable variability in disease progression between 5 and 10 months of age[38,39], 2) monthly cSLO *in vivo* imaging for long-term visualization of GFP+ cells in the retina and unmyelinated optic nerve of heterozygous *Cx3cr1*$^{GFP/+}$ DBA/2J mice aged 3-5 months, 3) live imaging analysis by segmentation and thresholding to isolate cell somata and measure their area. These strategies are applied to assess the kinetics of retinal microglial activation states during early stages of chronic glaucoma.

Protocol

In vivo imaging is performed in pathogen-free facilities using protocols approved by the Institutional Animal Care and Use Committee at the University of Utah.
NOTE: This imaging protocol is used for reporter mice in which retinal microglia and infiltrating monocytes/macrophages express green-fluorescent protein (GFP) under the control of the fractalkine receptor locus (CX3CR1).

1. *In Vivo* Imaging of Retinal GFP+ Microglia by Confocal Scanning Laser Ophthalmoscopy (cSLO)

1. Turn on the water-controlled heating system, set to stabilize mouse temperature between 35-37 ºC during procedure, and connect two heating pads.
    1. Start the confocal scanning laser ophthalmoscope (cSLO) system (**Figure 2A**). Open the cSLO program, enter the information that will identify the individual mouse and set a corneal curvature of 2 mm (Patient Data menu).
2. Prepare for imaging. Securely fit a clean 55º wide-field objective lens on its socket. Prepare the ophthalmoscope imaging platform by securing a heating pad covered with clean paper. Use clips to flatten the pad and paper and keep them from blocking the movement of the objective lens.
3. Anesthetize the mouse by intraperitoneal injection of 1.3% 2,2,2-tribromoethanol and 0.8% tert-amyl alcohol (250 mg/kg body weight; 0.5 ml/25 g body weight) using a 30½ G needle fitted to a 1 ml disposable syringe. Return mouse to its cage, kept over a heating pad.
   NOTE: The delivery of the anesthetic by injection versus inhalation allows easier positioning of the mouse for imaging and unobstructed access to the eyes, free of nose cones and tubing.
4. Once the animal stops moving and is unresponsive to tail pinch, induce pupil dilation with Tropicamide and phenylephrine (0.5% each), by positioning the animal prone and covering both eyes with the drops for 7 min.
5. After 5 min, place the mouse prone on the center of the ophthalmoscope platform, and fit contact lenses over both eyes, applying minimal pressure.
   NOTE: Contact lenses are small and fragile but can be carefully handled with fingers, although forceps can be used instead[40]. The use of contact lenses is optional, but recommended as it minimizes eye dryness and preserves corneal transparency during imaging.
6. After 7 min, orient the mouse with the right eye facing the objective lens and the orbit parallel to the objective lens, keeping the animal unrestrained near the edge of the platform (**Figure 2B**). To collect images of comparable saturation and orientation, constantly maintain the distance from eye to objective lens, as well as the alignment of the eye to the light path throughout imaging sessions. Clip long whiskers interfering with observation of the eye.
   NOTE: For the next 8-10 min, the mouse will not move or blink, and will breath with gentle movements, which are tracked by the cSLO Eye Tracking ART (automatic real time) mode, which adjusts the scan head position based on fundus landmarks with high contrast. Past that time, mice begin panting and blinking, making imaging impractical.
7. If imaging is performed without using contact lenses, apply PBS drops to both eyes every 2-3 min to prevent them from drying.
8. Collect a fundus image of the retinal vasculature and optic disc, focused on the inner retina.
    1. Select the infrared mode (IR) and adjust settings to 820 nm excitation, 100% laser power, 40-60% sensitivity (**Figure 2C**).
    2. Working in high-speed mode (12.6 frame/sec), locate the eye using the joystick to drive the ophthalmoscope. At low magnification, inspect the cornea and lens for injury or opacity, and exclude from the study eyes with defects or injury that will affect imaging the retina (**Figure 3A**).
    3. Locate the optic disc area (the surface of the optic nerve head, ONH) by bringing the objective closer to the eye, then center the image on it and lock this position by screwing the joystick. This alignment of the eye to the ophthalmoscope is key to obtain even focus and emission across the image.
    4. Visualize the inner planes of the retina, as well as the ONH, using the major blood vessels located on the vitreal surface of the retina as a reference focal plane (59 and 60 D), or deeper (55 D) in eyes showing excavated optic discs. The optimal focus should resolve circulating blood cells within major blood vessels, with their lumen and walls clearly distinct.
    5. Optimize image saturation by adjusting the dial on the touch screen control panel, until a white halo of uniform illumination spans in most of the 55º fundus field around the optic disc (using slight overexposure). Next, lower the saturation to optimize contrast until blood

cells moving along the major vessels can be clearly resolved. If focal dark areas persist, not due to retinal damage, realign the eye to the camera until a uniformly bright image is obtained. This adjustment is fundamental to capture reproducible sets of images in position and quality.

6. Collect a high-resolution IR image of the central retina (1.4-1.7 mm in diameter, depending on age), averaging 30 frames in real time (4.7 frames/sec; normalized), to improve signal-to-noise ratio (**Figure 2D**).

9. Immediately, acquire a fluorescence image of GFP+ microglia and/or infiltrating monocytes localized to the inner planes of the retina and the ONH.
   NOTE: Optimization of the IR fundus image of the retina determines the resolution of the fluorescence image of GFP+ cells, as well as the extent of inner retina spanned. Failure to focus the inner planes of the retina, which can be detected by poor resolution of the vasculature, will result in dimmed GFP+ cell views (**Figure 3B**). Failure to adjust IR saturation correctly and uniformly affects the fluorescence image (FA), introducing artifactual variations in GFP+ cell intensity and size (**Figure 3C**).
   1. Swich to fluorescence imaging mode (FA) in the touch screen panel, using blue, 488 nm laser excitation (460-490 nm barrier filter set), and acquisition settings (100% laser power and 100-125% sensitivity), which are maintained constant for all mice (**Figure 2E**).
   2. Collect a single xy-point, bidimensional fluorescence image of the retina, and immediately capture a fundus image at identical position (100x scan average; 55º scan angle for both images; **Figure 2F**).
   3. Capture a multipoint image by selecting “composite” in the control panel (**Figure 2G**) and moving the ophthalmoscope right and left, panning the retina across the nasal-temporal axis (**Figure 2H**).
      NOTE: After scanning a single xy-point image (100x scan average), the software automatically averages new scans of the same and new areas (circumscribed with a green circle during optimal scan, or red when the scan is unfeasible), and stitches all xy-positions in real time. The resulting composite image spans 1.5-1.7 mm on the horizontal axis x 3-4 mm in the vertical axis (55º x 120-124º scan angle).

10. Complete imaging of each mouse within 15 min after inducing anesthesia, before blinking and motion restarts.
11. Remove contact lenses, hydrate eyes with PBS and return the animal to its warmed cage, checking behavior until full recovery of motility.
12. For longitudinal studies using intermittent cSLO-imaging sessions in the same individual mouse, repeat imaging no less than 3 days apart to avoid the cumulative toxicity of anesthesia, as well as corneal irritation.

2. Live Image Processing and Analysis

1. Sequential image alignment:
   1. Align the fundus images for a time series of the same eye using the vasculature and optic disc as landmarks. Open all images in a commercial slide-show presentation program, by dragging each image over the preceding one until their optic discs align on the *xy*-plane (the top image appears semi-transparent while being dragged), then rotate the top image until its major blood vessels overlap with the vasculature on the image below (focus on vessels farthest from the optic disc). Record the rotation angle for each image and save this time series for future reference, keeping track of mouse and eye identity.
   2. Align the corresponding series of single xy-point fluorescence images by applying the recorded angle to correct the *x*-*y* rotation at each time point, using a raster graphic editor program. Additionally, adjust resolution to 300 dpi (without rescaling) and background (in the RGB mode, select Levels and sample the lumen of a blood vessel as black). Save these images as TIF files, adding “aligned” to their names.

2. Microglial cell segmentation:
   1. To identify GFP+ cells in the central retina, open in FluoRender the “aligned” TIF file corresponding to the earliest time point/age. Zoom the image to fit the screen, then define the Render view (composite, orthogonal, interpolated) and its properties (0.58 gamma, 255 saturation point, 255 luminance, 195 alpha and 1.00 shading), selecting both the RG channels as visible (hide B channel by double-clicking it in the Workspace frame; **Figure 4A**).
   2. To select individual cells, threshold the red channel (must be highlighted on the Workspace frame), by increasing the low threshold until the majority of cells are masked (white) with minimum overlap and cell processes (cyan), while keeping the high threshold constant (255). The low threshold value varies between 100 and 170, depending on the fluorescence intensity (**Figure 4B**).
   3. Save this view with the red channel visible only (Capture command) as a new TIF file, adding “cellsegm” to its original name (**Figure 4C**). Using a generic raster graphic editor software, invert its greyscale and adjust resolution to 300 dpi as above, and save again as RGB (**Figure 4D**).
      NOTE: Delete the folders (projects) automatically created by FluoRender, and save the applied threshold for future reference.

3. Microglial soma segmentation and morphometry:
   1. To identify GFP+ cell somata for area quantification, use image analysis software with automated intensity measurements and threshold capabilities, as well as threshold-based object counting and measurement. Open the “cellsegm” TIF file, and select the rescaling method (spline) and the red channel (click red tab in RGB). Improve visualization by deselecting “view channel in color” (right-click the red RGB tab), and selecting “complement colors” (Image/Adjust Image) to invert the greyscale and see the cells in grey/black over white background (**Figure 4E**).
   2. Calibrate the image to 1.4-1.7 mm depending on age, by drawing a horizontal line across the entire image (Calibration, Quick Calibration).
   3. Segment individual cell somata by applying intensity thresholding (**Figure 4B**). For this, work on the red RGB channel and open the Threshold Intensity function (Object Count; selecting “count update” command) in order to track bidimensional parameters for each thresholded region of interest (ROI) representing individual somata.
   4. Define the intensity threshold in the intensity histogram, by selecting the lowest 50-60% of the 255 levels, and refining the final threshold value by visually assessing the overlap between the threshold color mask (blue) and the cell soma perimeter (grey) in individual cells (**Figure 4E**).

5. Estimate the accuracy of the cell soma masks to represent the somal dimensions by measuring the area before and after segmentation in 10 cells and accept the selected threshold range if the measurements differ less than 10% (use the Binary Toolbar and Annotated Measurements).
6. Manually identify somal ROIs that include multiple cells and separate these elements (eliminate or separate ROIs using the Binary Toolbar controls, or the Object Catalog) while toggling on/off the binary to directly visualize the cells (**Figure 4F**).
7. Classify microglial cells as ROIs with somal areas larger and smaller than 50-60 μm^2 to discriminate cell somata corresponding to activated microglia and deactivated microglia respectively, by using Area Restriction.
   NOTE: Each cell somal subset is identified with a different pseudocolored binary layer, and can be further characterized for other morphological parameters (perimeter, circularity, *etc.*), as well as quantified within discrete retinal sectors (**Figure 4G**). Save the analyzed image as an ND2 file.
8. Verify the process and branching complexity in individual activated microglial cells, by overlaying the somal mask and the single *xy*-point image (contrast increased 50%; **Figure 4H**). Manually count the processes directly extending from the cell soma or measure the diameter of the polygon encompassing the arbor (use the Binary Toolbar and Annotated Measurements).
   NOTE: Activated cells lack processes or bear few (<4) and short (<2x somal diameter) ones, in contrast to non-activated cell processes, which comprise a ramified and extensive arbor (> 3-10x somal diameter) surrounding their relatively small soma.
9. Manually identify cells with somata smaller than <20 μm^2 and/or GFP expression below the detection limit, which are therefore undetected by intensity thresholding. Use the Taxonomy command in Annotations to count manually identified elements.

Representative Results

Our recent *in vivo* studies used these live image acquisition and analysis methods to visualize and track the kinetics and patterns of ONH and retinal microglial changes during early stages of chronic glaucoma and their relationship to late neurodegeneration[59]. Here we illustrate a cSLO image acquisition protocol to visualize microglial cells across a large area of the central retina in individual young heterozygous Cx3CR1-GFP DBA/2J retinas (**Figure 5**). Based on the high cell resolution, we apply live image thresholding and morphometric analyses that allow the automatic segmentation of individual GFP+ cells and somata (**Figure 6**).

To monitor the development of local microgliosis and/or microglia activation at ages preceding detectable neurodegeneration in this model of chronic glaucoma, we measured monthly variations of total microglia cell density in individual young heterozygous Cx3CR1-GFP DBA/2J retinas (n = 10) between 3-5 months of age (**Figure 7A**). Consistent with the variable progression of neurodegeneration in individual eyes[41-44], our analysis reveals variable levels of retinal microglia activation and microgliosis across eyes at each age (**Figure 7B**), and detects dynamic changes in the density of total and activated microglia within individual retinas (**Figure 7C**). Noticeably, numbers of activated microglia are uncoupled from concurrent changes in total GFP+ cell density. These *in vivo* findings confirm previous *ex vivo* analysis of microglial changes in DBA/2J mice[45]. Thus cSLO live detection and measurement of retinal microglial activation may serve as indicators of early disease progression within individual eyes, and may potentially be linked to initiating events of glaucoma pathogenesis.

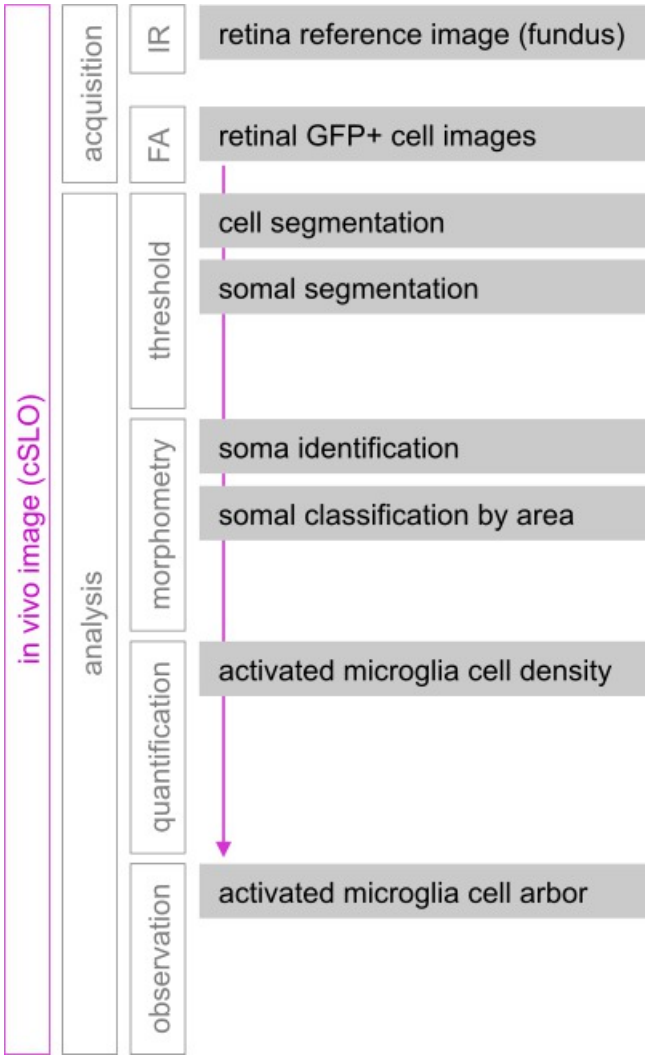

Figure 1: Live image acquisition, processing and analysis workflow. cSLO was used to image hundreds of GFP+ microglial/peripheral monocyte cells localized to the central ~1.7 mm^2 of the mouse inner retina. Fluorescence images (FA) were acquired monthly for the same mice, and aligned using infrared (IR) fundus images of the retinal vasculature and vitreal surface as reference. Segmentation of GFP+ cells and somata resulted from applying two separate steps of intensity-thresholding to FA retinal images. Morphometric analysis of the binary representing cell somata allowed measurement of individual somal areas. GFP+ cells with somal area above 50 μm^2 were classified as activated. Density of total and activated GFP+ cells was measured for individual retinal FA images, and examination of arbor extension and branching complexity was performed by direct observation of FA images.

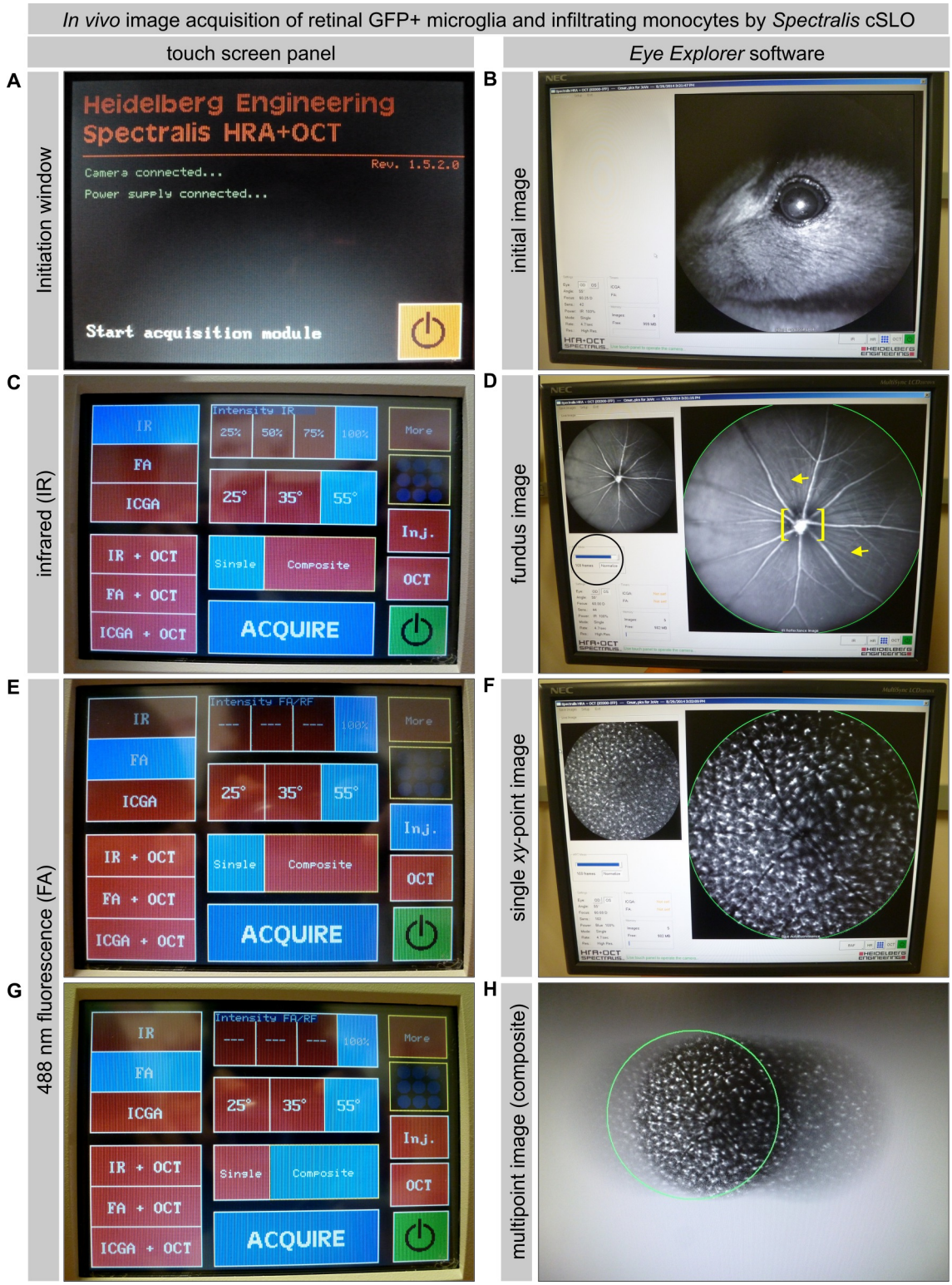

Figure 2: Live image acquisition controls in cSLO Spectralis. (**A**) Manual touch screen panel display on initiation. (**B**) *cSLO software* imaging window, showing the head of a live mouse. (**C**) Settings selected for infrared imaging (lit in blue). (**D**) Fundus image of the retina during real time acquisition (left panel) and average (right panel). Normalization command indicated with black circle. Arteries and veins radiating from the optic nerve head are visible (between brackets), as are the optic axonal bundles (arrows) in between the blood vessels. (**E**) Settings selected for fluorescence imaging within a single *xy* point. (**F**) Single-point fluorescence (FA, 488 nm) imaging during acquisition (averaging). The smaller image (left) shows an individual scan, the larger image (right) shows the progress of intensity averaging. (**G**) Settings selected for acquisition of a multipoint (composite), fluorescence image. (**H**) Multipoint fluorescence imaging acquisition, showing the scan in progress, which the software identifies with a green circle (or red when acquisition is not possible). Scale bars represent ~5 mm (B) or 250 µm (D-H) Please click here to view a larger version of this figure..

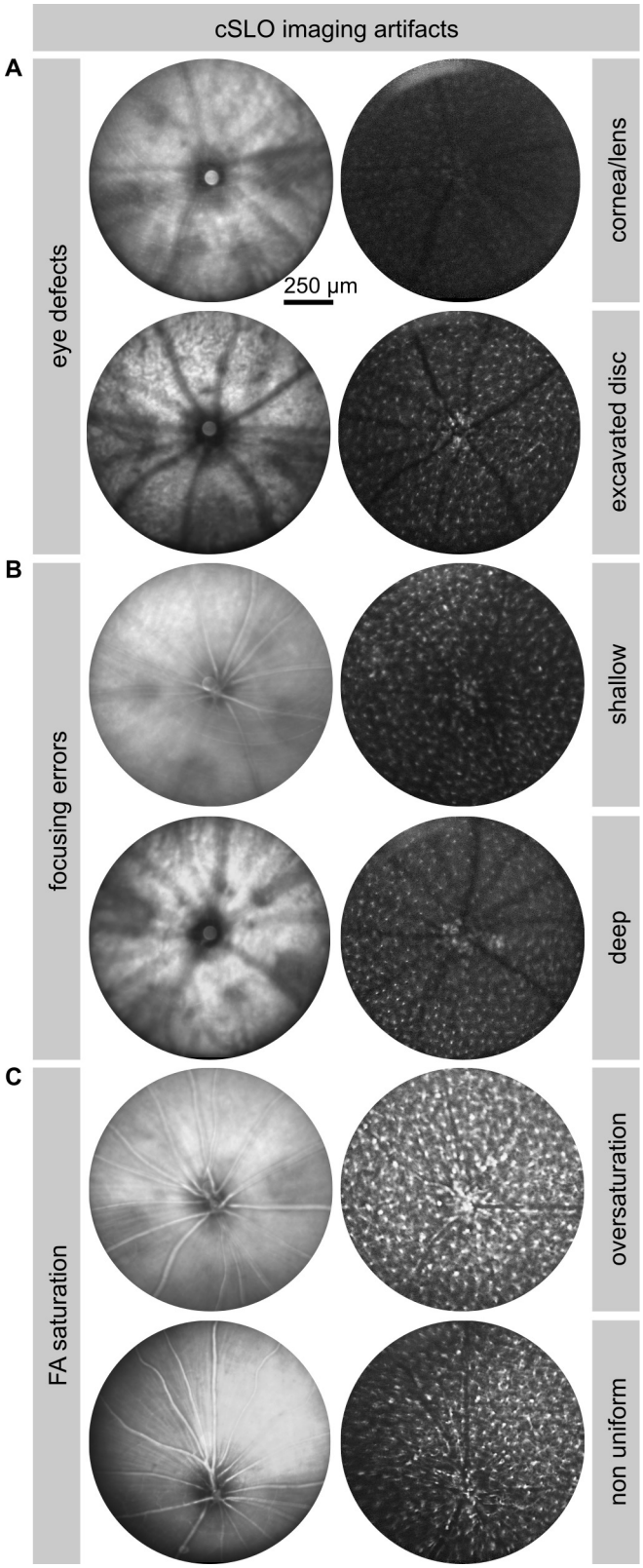

Figure 3: Key ocular defects and imaging errors that can prevent correct cSLO imaging of microglial cells. (**A**-**C**) Ocular damage or defects, as well as image acquisition errors can prevent reliable imaging of GFP+ cells localized to the innermost planes of the retina. (**A**) Some gross eye defects are readily detectable in fundus images, including corneal or lens opacity, or injury and deepening of the optic disc area, all of which prevent clear imaging of GFP+ cells. (**B**) Focusing either above (the walls of the vessels become indistinguishable from the lumen) or below the inner surface of the retina (the vessels are barely visible) reduces the detectability of GFP fluorescence emission from cells located at the nerve fiber and ganglion cell layers. (**C**) Saturation levels incorrectly or unevenly set can result in bright but oversaturated images (with cells lacking resolution) or images with obscured areas. Scale bar represents 250 µm. Please click here to view a larger version of this figure.

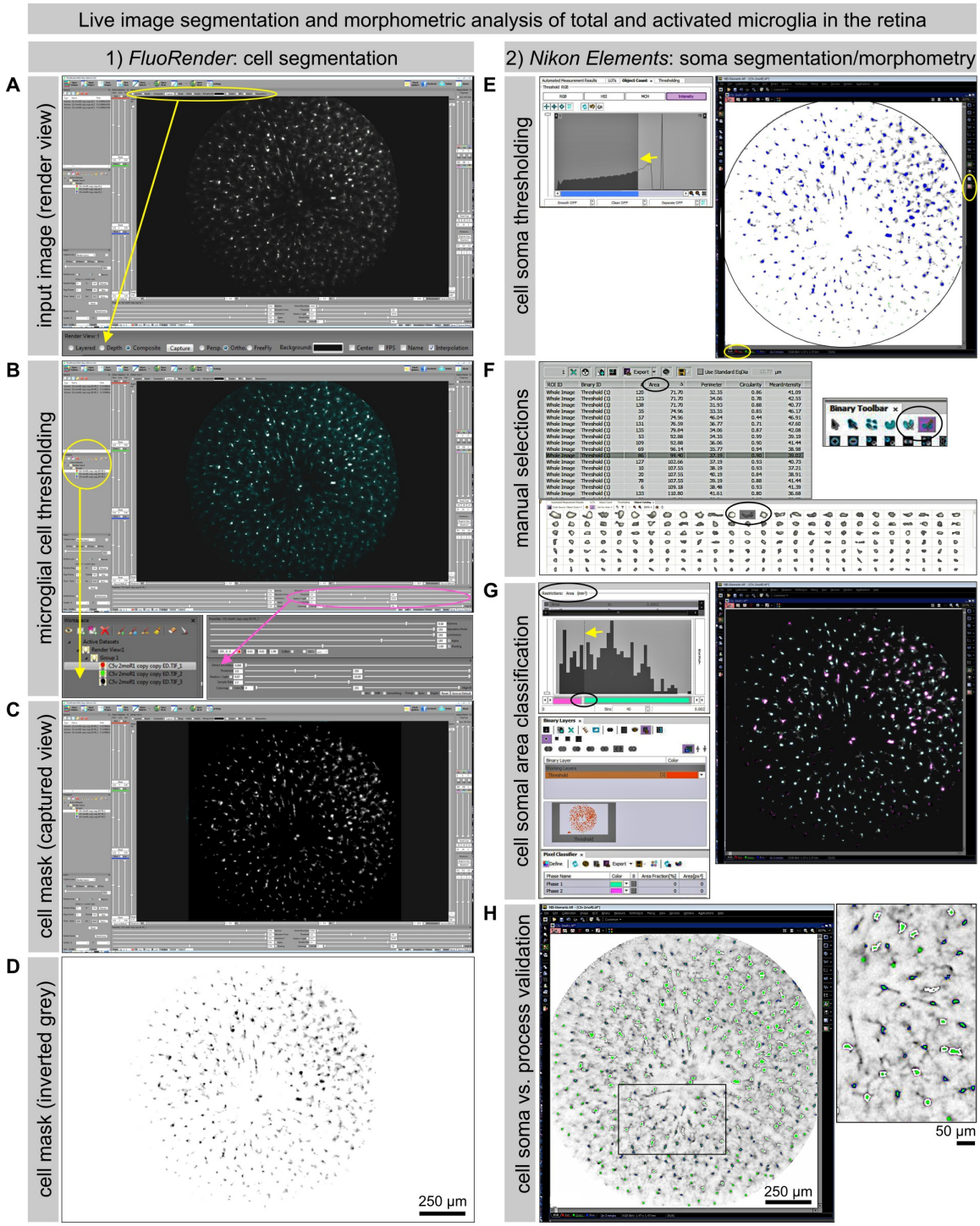

Figure 4: Binary thresholding-based quantification of microglial cell counts and somal area. (**A**-**D**) Steps of cell segmentation in *FluoRender.* (**A**) Navigation window with rendered view of a representative single-point fluorescence image of microglia within the central retina (top panel); corresponding rendering properties (lower panel). (**B**) The same image during a cell segmentation routine, viewed as RGB, with corresponding threshold settings (lower panels). Thresholded cells are represented by white pixels and overlaid to their processes in cyan. (**C**) Image of cell masks obtained after cell segmentation. (**D**) Previous mask with inverted greyscale values for further image processing. (**E**-**H**) Steps of somal thresholding and quantification. (**E**) Use of intensity threshold to segment microglia somata based on their previous cell segmentation. The RGB intensity histogram (left) allows thresholding by direct selection of the lower 50-60% range of intensities (0 to 127-153). This segmentation creates a quantifiable mask that isolates individual microglial somata (blue). Images are rescaled using the spline function (oval at right). (**F**) Automatic threshold-based measurements of individual ROI/somata (top panel) and ROI silhouettes (Object Catalog, bottom panel) used to correct overlapping ROIs using Binary Tools (right panel) for manual separation or erosion. (**G**) Classification of individual somal areas by Area Restriction (top left panel). Segmented somata are classified as ROIs smaller and larger than 50-60 μm^2, and the binary layers for each class of somata are assigned different color pixels (green and magenta, respectively). (**H**) Overlay of the segmented somata (green) on the original image (with increased contrast) used for direct observation of process complexity in individual activated cells (left panel). Magnified view of cell arbors. Scale bars represent 250 µm (A-H) or 50 µm (H, inset). Please click here to view a larger version of this figure.

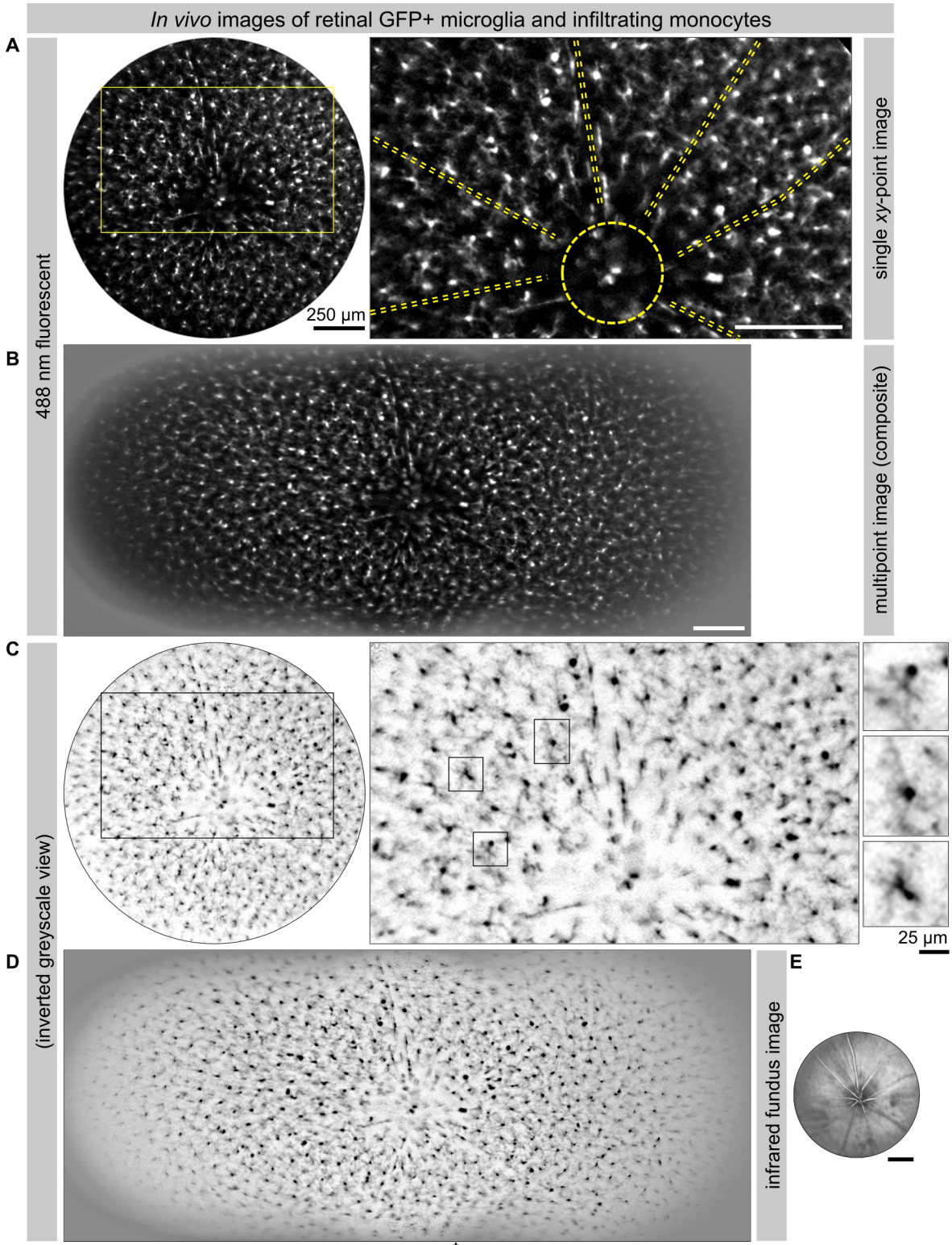

Figure 5: High-resolution visualization of *CX3CR1*-GFP$^+$ microglia/monocytes localized to the inner mouse retina by live confocal scanning laser imaging. (**A**) Single *xy*-point cSLO image showing GFP$^+$ cells within the central retina in a 2 month old DBA/2J mouse (left). Magnified view (right) showing the ONH area (circle), blood vessels (lines) lined with perivascular microglia/macrophages, and parenchymal microglia tiling the central retina. (**B**) Multipoint image, collected immediately after the single point to visualize microglia across a wider retinal area (⅓ of the retina). (**C**, **D**) Identical images, shown with inverted greyscale for optimal observation of cell morphology and complexity (minimally adjusted for contrast and resolution). Somal size and shape can be resolved in most cells (left). Arbor extension and cell branching can be resolved in the cells with large somata (right, and 3 individual cells). (**E**) Infrared fundus image of the vasculature and optic disc used for *xy*-plane alignment of sequential images. Scale bars represent 250 µm (A, B and E), and 25 µm (C, far right). Please click here to view a larger version of this figure.

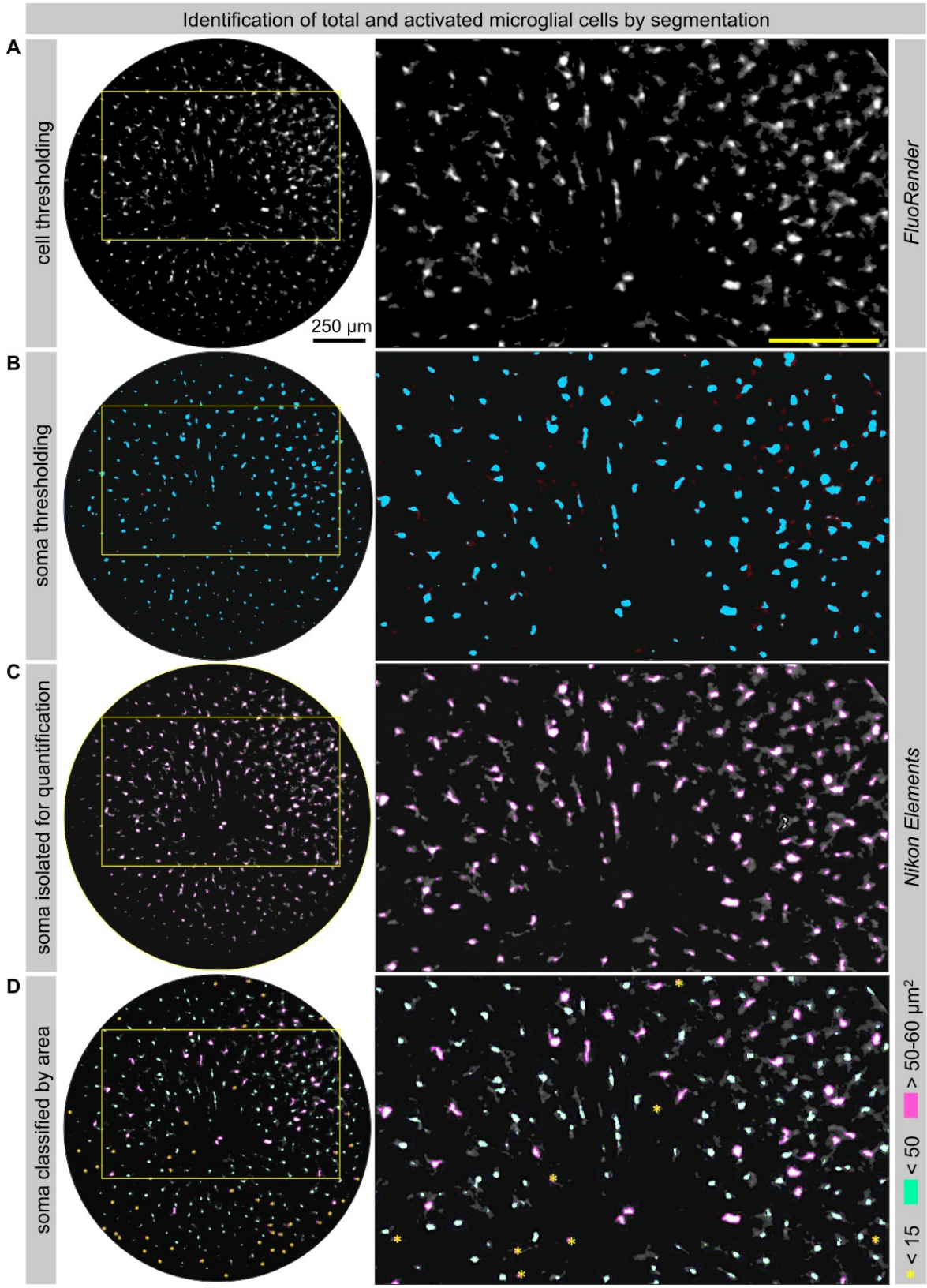

Figure 6: Segmentation of microglial cell and somata. (**A**) GFP+ cells rendered by segmentation in 2D using *FluoRender*. (**B**) Corresponding cell somata, detected by thresholding using confocal image analysis software. (**C**) Binary mask of cell somata amenable to quantitative analysis. (**D**) Classification of segmented cell somata by area to discriminate activated microglial cells (>50-60 µm^2, magenta), and non-activated cells (<50 µm^2, green). Dim and small cells (<10-20 µm^2, yellow asterisk) are identified manually in the original image with inverted greyscale (**Figure 3C**). Scale bars represent 250 µm. Please click here to view a larger version of this figure.

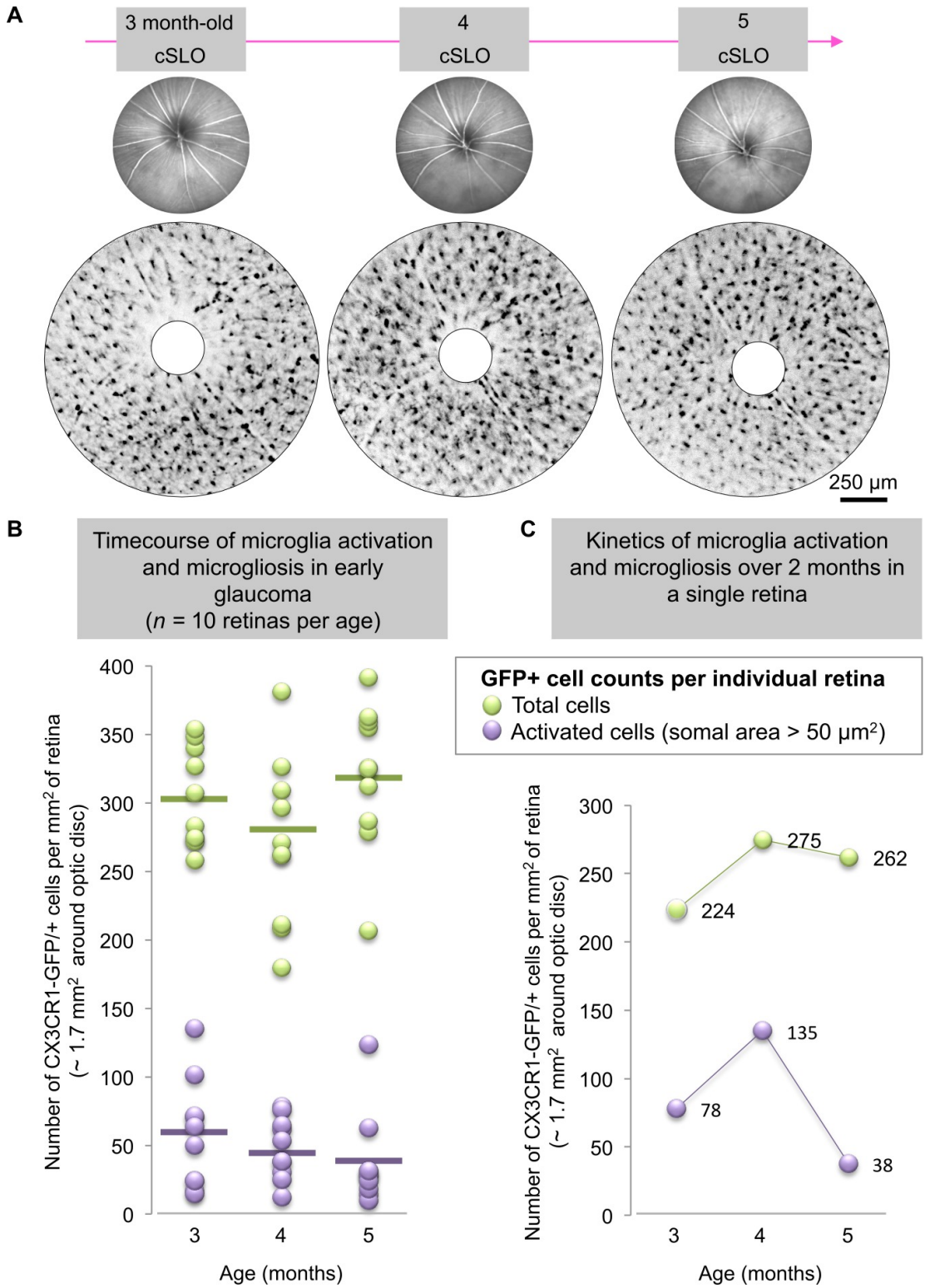

Figure 7: Longitudinal tracking of microglial cell density and activation in young DBA/2J retinas. (**A**) Live cSLO fundus and FA images of the same eye, acquired from 3-5 months of age. Sequential FA images were used to quantify changes over time in total numbers of CX3CR1-GFP$^+$ cells localized within the central ~1.7 mm^2 of retina. Counts included parenchymal and perivascular microglia, but excluded cells clustered at the ONH (position indicated with white circle). (**B**) Timecourse analysis of retinal microglia cell density and activation at ages preceding neurodegeneration in DBA/2J chronic glaucoma (*n* = 10 retinas per age). Numbers of total GFP+ cells and of activated microglial cells (somal area >50 µm^2) per mm^2 of central retina. Each data point represents a single retina, and means for each age are represented with a horizontal line. (**C**) Monthly tracking of numbers of total GFP+ cells and of activated microglial cells in a single retina. There are parallel but quantitatively different changes in total and activated cell density, with more dynamic variation in the density of morphologically activated cells. Scale bar represents 250 µm (A). Please click here to view a larger version of this figure.

Discussion

Live monitoring of microglial cell number and morphological activation during a neurodegenerative disease requires the use of non-invasive imaging methods that allow the detailed visualization of cell features. After imaging, microglial cells must be isolated (segmented) for morphometric analysis by use of multiple threshold steps to assess somal size and/or process complexity as readouts for microglia activation. In this protocol, we describe methods for live image acquisition using cSLO, and quantitative analysis of microglial activation based on sequential cell and soma segmentation. We apply these strategies to assess the kinetics of retinal microglia activation and microgliosis over 2 months in the context of a chronic neurodegenerative disease of the retina.

Reporter mice and microglia/peripheral monocytes cell types

The use of mice that express GFP under the control of the fractalkine receptor (CX3CR1) locus[46] allows reliable identification of resident microglia, and robust GFP expression permits remarkable *in vivo* visualization[30-32,34,36]. Here, we use a substrain of DBA/2J mice, derived by backcrossing C57BL/6.129P-*Cx3cr1* ^{tm1Litt}/J mice[46] into the DBA/2J genetic background[59]. Peripheral monocytes and macrophages, which can invade the CNS during disease or injury, also express the GFP tag[15,46,47].

Live imaging studies of microglia in the neurodegenerative retina

Our *in vivo* tracking of CX3CR1-GFP/+ retinal cells using cSLO builds on previous studies that monitored changes in retinal GFP+ cell numbers following acute injury for up to 10 weeks[30-32,34,48]. Here, we visualize CX3CR1-GFP/+ microglia/peripheral monocytes with cellular resolution, by monthly cSLO imaging of the retina during the early progression of chronic glaucoma. Additionally, we use live image automated threshold-based analysis to detect and quantify cell resizing and remodeling with enough spatial and temporal resolution to monitor changes in activated and total microglia counts within individual eyes and across individuals.

Technical limitations of cSLO imaging of GFP+ microglia in the retina

We found imaging quality to be consistent and reproducible, as illustrated by a comparison of single versus multi-*xy* point images obtained in a single session (**Figure 5**). However, consistent and reproducible GFP+ cell imaging acquisition, in a single session and over time, is critically depend on the selection of stable parameters for fundus and fluorescence cSLO imaging. Alignment of the eye and optic disc to the cSLO objective determines the uniformity of saturation levels and the focus on the confocal plane of interest[49]. Inaccurate and/or non-uniform specification of saturation levels can generate artifactual variations in GFP detection, autofluorescence background, and cell and arbor resolution. To correctly focus on microglia localized to the nerve fiber and ganglion cell layers, it is critical to align and focus on the retinal blood vessels and on axonal bundles at the vitreal surface by IR fundus imaging. This provides a reference plane to locate the GFP+ cells by FA. The required refocusing needed for switching from IR to FA can be guided by the acquisition of multiple FA images at slightly different depths (55-60 D) in each experimental session. This can also help compensate for anatomical differences due to age, pupil dilation and pathology (optic disc excavation). Since image resolution and cell detail depends on the optimal specification of saturation levels throughout the fundus, and careful alignment of the eye relative to the camera[49], image sequences acquired over time for the same eye must show fundus IR images with consistent and comparable focus, illumination, resolution and retinal field span. Manual counts of total GFP+ cell numbers in images acquired in a single session (1.5-1.7 mm^2 of retina, n = 13 retinas, aged 3-5 months) confirmed consistent and reproducible quantification of cellularity (3-4% variation; data not shown). This is necessary for images to be amenable for GFP+ cell segmentation via threshold analysis based on a similar intensity range, and comparison of changes over time.

Threshold and morphometric analyses of retinal microglia in live cSLO images

Only recently, *in vivo* visualization of brain microglia with high cellular resolution by two-photon confocal microscopy has enabled the quantitative analysis of microglial soma and process parameters, and the discrimination of morphologically activated microglia[9,50]. As shown by these authors, somal size is the most conspicuous morphological parameter detectable over time by live two-photon confocal imaging of brain microglia, using iterative intensity-based thresholding to reduce signal-to-noise variations[9]. Furthermore, somal size changes correlate with upregulation of Iba1 expression in activated cells[9]. Here, we use cSLO live images and apply comparable sequential segmentation of microglial cells and somata, followed by morphometric analysis to quantify numbers of total and activated CX3CR1-GFP+ cells localized to the retina.

We use specialized confocal rendering software (FluoRender) to segment GFP+ cells in the central retina. These images, are further thresholded using a commercially available confocal image analysis package, to ultimately allow the automatic segmentation and threshold-based quantification of somal area. Our live image analyses confirmed the use of soma size as a morphological metric of microglial activation in live image analysis[9]. Somal threshold-based counts allowed the characterization of patterns and increases in retinal microgliosis, as previously demonstrated by *ex vivo* image analysis[50]. We find that cSLO detects GFP+ microglia with best resolution and detail within the mouse central retina (<2 mm^2), where cells can be imaged at the same confocal plane. Towards the retina periphery, the fluorescence signal shows variability and distortions that prevent identical imaging processing and threshold analysis as for GFP+ cells detected in the flatter central retina. Finally, our protocol shows that cSLO *in vivo* image analysis of retinal microglia offers a relatively high throughput. The number of parenchymal microglial that could be visually isolated and quantified within the central retina varied between ~200-300 total cells, and ~10-180 activated cells. Thus, the mouse retinal microglia offers an optimal population to study *in vivo* their transformation and roles during the pathogenesis of neurodegeneration.

Application to other CNS chronic diseases

The *in vivo* image analysis methods described here should be applicable to assess acute or chronic microglial changes in other mouse retinal diseases and injury models. Furthermore, this protocol may serve to evaluate retinal microglia/peripheral monocyte changes resulting from chronic CNS pathologies, such as Alzheimer's, Parkinson's and multiple sclerosis, given that the retina and optic nerve are targeted for neurodegeneration in these diseases[51-56]. In line with this, the use of live detection of retina and ONH pathology for early Alzheimer's disease management is under intense study[54,57,58].

In conclusion, our findings suggest that live, longitudinal tracking and quantification of changes in retinal microglia numbers and morphological activation, may serve as reliable neuroimaging biomarkers to detect disease onset and early progression. These *in vivo* imaging and analysis methodology apply to age-related glaucoma, and potentially to other neurodegenerative diseases that impact the retina and optic nerve.

Disclosures

The authors have nothing to disclose.

Acknowledgements

We thank the Scientific Computing and Imaging Institute of the University of Utah for use of *FluoRender* software (R01GM09815). This work was supported by grants from the Glaucoma Research Foundation, Melsa M. and Frank Theodore Barr Foundation and the US National Institute of Health, (R01EY020878 and R01EY023621) to M.L.V., and (R01EY017182 and R01EY017950) to B.K.A.

References

1. Hanisch, U. K. Functional diversity of microglia - how heterogeneous are they to begin with. *Front. Cell. Neurosci.* **7**, (65), 1-18 (2013).
2. Kettenmann, H., Hanisch, U. K., Noda, M., Verkhratsky, A. *Physiology of microglia. Physiol. Rev.* **91**, (2), 461-553 (2011).
3. Davalos, D., *et al.* ATP mediates rapid microglial response to local brain injury in vivo. *Nat. Neurosci.* **8**, (6), 752-758 (2005).
4. Nimmerjahn, A., Kirchhoff, F., Helmchen, F. Resting microglial cells are highly dynamic surveillants of brain parenchyma in vivo. *Science.* **308**, (5726), 1314-1318 (2005).
5. Ransohoff, R. M., Perry, V. H. Microglial physiology: unique stimuli, specialized responses. *Annu. Rev. Immunol.* **27**, 119-145 (2009).
6. Stence, N., Waite, M., Dailey, M. E. Dynamics of microglial activation: a confocal time-lapse analysis in hippocampal slices. *Glia.* **33**, (3), 256-266 (2001).
7. Streit, W. J., Walter, S. A., Pennell, N. A. Reactive microgliosis. *Prog. Neurobiol.* **57**, (6), 563-581 (1999).
8. Jonas, R. A., *et al.* The spider effect: morphological and orienting classification of microglia in response to stimuli in vivo. *PloS One.* **7**, (2), e30763 (2012).
9. Kozlowski, C., Weimer, R. M. An automated method to quantify microglia morphology and application to monitor activation state longitudinally in vivo. *PloS One.* **7**, (2), 1-9 (2012).
10. Ajami, B., Bennett, J. L., Krieger, C., Tetzlaff, W., Rossi, F. M. Local self-renewal can sustain CNS microglia maintenance and function throughout adult life. *Nat. Neurosci.* **10**, (12), 1538-1543 (2007).
11. Elmore, M. R., *et al.* Colony-stimulating factor 1 receptor signaling is necessary for microglia viability, unmasking a microglia progenitor cell in the adult brain. *Neuron.* **82**, (2), 380-397 (2014).
12. Lawson, L. J., Perry, V. H., Dri, P., Gordon, S. Heterogeneity in the distribution and morphology of microglia in the normal adult mouse brain. *Neuroscience.* **39**, (1), 151-170 (1990).
13. Ransohoff, R. M., Cardona, A. E. The myeloid cells of the central nervous system parenchyma. *Nature.* **468**, 253-262 (2010).
14. Solomon, J. N., *et al.* Origin and distribution of bone marrow-derived cells in the central nervous system in a mouse model of amyotrophic lateral sclerosis. *Glia.* **53**, 744-753 (2006).
15. Ajami, B., Bennett, J. L., Krieger, C., McNagny, K. M., Rossi, F. M. Infiltrating monocytes trigger EAE progression, but do not contribute to the resident microglia pool. *Nat. Neurosc.* **14**, (9), 1142-1149 (2011).
16. Sapp, E., *et al.* Early and progressive accumulation of reactive microglia in the Huntington disease brain. *J. Neuropathol. Exp. Neurol.* **60**, (2), 161-172 (2001).
17. Maeda, J., *et al.* In vivo positron emission tomographic imaging of glial responses to amyloid-beta and tau pathologies in mouse models of Alzheimer's disease and related disorders. *J. Neurosc.* **31**, (12), 4720-4730 (2011).
18. Jacobs, A. H., Tavitian, B. Noninvasive molecular imaging of neuroinflammation. *J. Cereb. Blood Flow Metab.* **32**, (7), 1393-1415 (2012).
19. Ouchi, Y., *et al.* Microglial activation and dopamine terminal loss in early Parkinson's disease. *Ann. Neurol.* **57**, (2), 168-175 (2005).
20. Fuhrmann, M., *et al.* Microglial Cx3cr1 knockout prevents neuron loss in a mouse model of Alzheimer's disease. *Nat. Neurosci.* **13**, (4), 411-413 (2010).
21. Trapani, A., Palazzo, C., de Candia, M., Lasorsa, F. M., Trapani, G. Targeting of the translocator protein 18 kDa (TSPO): a valuable approach for nuclear and optical imaging of activated microglia. *Bioconjug. Chem.* **24**, (9), 1415-1428 (2013).
22. Venneti, S., Lopresti, B. J., Wiley, C. A. Molecular imaging of microglia/macrophages in the brain. *Glia.* **61**, (1), 10-23 (2013).
23. Davalos, D., *et al.* Fibrinogen-induced perivascular microglial clustering is required for the development of axonal damage in neuroinflammation. *Nat. Comm.* **3**, (1227), 1-15 (2012).
24. Dibaj, P., *et al.* In Vivo imaging reveals distinct inflammatory activity of CNS microglia versus PNS macrophages in a mouse model for ALS. *PloS One.* **6**, (3), e17910 (2011).
25. Evans, T. A., *et al.* High-resolution intravital imaging reveals that blood-derived macrophages but not resident microglia facilitate secondary axonal dieback in traumatic spinal cord injury. *Exp. Neurol.* **254**, (214), 109-120 (2014).
26. Nayak, D., Zinselmeyer, B. H., Corps, K. N., McGavern, D. B. In vivo dynamics of innate immune sentinels in the CNS. *Intravital.* **1**, (2), 95-106 (2012).
27. Tremblay, M. E., Lowery, R. L., Majewska, A. K. Microglial interactions with synapses are modulated by visual experience. *PLoS Biol.* **8**, (11), 1-16 (2010).
28. Wake, H., Moorhouse, A. J., Jinno, S., Kohsaka, S., Nabekura, J. Resting microglia directly monitor the functional state of synapses in vivo and determine the fate of ischemic terminals. *J. Neurosci.* **29**, (13), 3974-3980 (2009).
29. Marker, D. F., Tremblay, M. E., Lu, S. M., Majewska, A. K., Gelbard, H. A. A thin-skull window technique for chronic two-photon in vivo imaging of murine microglia in models of neuroinflammation. *J. Vis. Exp.* **19**, (43), (2010).
30. Alt, C., Runnels, J. M., L, T. G. S., P, L. C. In vivo tracking of hematopoietic cells in the retina of chimeric mice with a scanning laser ophthalmoscope. *Intravital.* **1**, (2), 132-140 (2012).

31. Eter, N., *et al.* In vivo visualization of dendritic cells, macrophages, and microglial cells responding to laser-induced damage in the fundus of the eye. *Invest. Ophthalmol., & Vis. Sci.* **49**, (8), 3649-3658 (2008).
32. Liu, S., *et al.* Tracking retinal microgliosis in models of retinal ganglion cell damage. *Investigative ophthalmology & visual science.* **53**, 6254-6262 (2012).
33. Maeda, A., *et al.* Two-photon microscopy reveals early rod photoreceptor cell damage in light-exposed mutant mice. *Proc. Natl. Acad. Sci. USA.* **111**, (14), E1428-E1437 (2014).
34. Paques, M., *et al.* High resolution fundus imaging by confocal scanning laser ophthalmoscopy in the mouse. *Vision Res.* **46**, (8-9), 1336-1345 (2006).
35. Seeliger, M. W., *et al.* In vivo confocal imaging of the retina in animal models using scanning laser ophthalmoscopy. *Vision Res.* **45**, (28), 3512-3519 (2005).
36. Alt, C., Runnels, J. M., Mortensen, L. J., Zaher, W., Lin, C. P. In vivo imaging of microglia turnover in the mouse retina after ionizing radiation and dexamethasone treatment. *Invest. Ophthalmol., & Vis. Sci.* **55**, (8), 5314-5319 (2014).
37. Bosco, A., *et al.* Reduced retina microglial activation and improved optic nerve integrity with minocycline treatment in the DBA/2J mouse model of glaucoma. *Invest. Ophthalmol., & Vis. Sci.* **49**, (4), 1437-1446 (2008).
38. Anderson, M. G., *et al.* Mutations in genes encoding melanosomal proteins cause pigmentary glaucoma in DBA/2J mice. *Nat. Genet.* **30**, (1), 81-85 (2002).
39. Chang, B., *et al.* Interacting loci cause severe iris atrophy and glaucoma in DBA/2J mice. *Nat. Genet.* **21**, (4), 405-409 (1999).
40. Smith, R. S., Korb, D., John, S. W. A goniolens for clinical monitoring of the mouse iridocorneal angle and optic nerve. *Mol. Vis.* **8**, 26-31 (2002).
41. Buckingham, B. P., *et al.* Progressive ganglion cell degeneration precedes neuronal loss in a mouse model of glaucoma. *J. Neurosci.* **28**, (11), 2735-2744 (2008).
42. Howell, G. R., *et al.* Axons of retinal ganglion cells are insulted in the optic nerve early in DBA/2J glaucoma. *J. Cell Biol.* **179**, (7), 1523-1537 (2007).
43. Jakobs, T. C., Libby, R. T., Ben, Y., John, S. W., Masland, R. H. Retinal ganglion cell degeneration is topological but not cell type specific in DBA/2J mice. *J. Cell Biol.* **171**, (2), 313-325 (2005).
44. Soto, I., *et al.* Retinal ganglion cells downregulate gene expression and lose their axons within the optic nerve head in a mouse glaucoma model. *J. Neurosci.* **28**, (2), 548-561 (2008).
45. Bosco, A., Steele, M. R., Vetter, M. L. Early microglia activation in a mouse model of chronic glaucoma. *J. Comp. Neurol.* **519**, (4), 599-620 (2011).
46. Jung, S., *et al.* Analysis of fractalkine receptor CX(3)CR1 function by targeted deletion and green fluorescent protein reporter gene insertion. *Mol. Cell. Biol.* **20**, (11), 4106-4114 (2000).
47. Broux, B., *et al.* CX(3)CR1 drives cytotoxic CD4(+)CD28(-) T cells into the brain of multiple sclerosis patients. *J. Autoimmun.* **38**, (1), 10-19 (2012).
48. Paques, M., *et al.* In vivo observation of the locomotion of microglial cells in the retina. *Glia.* **58**, (14), 1663-1668 (2010).
49. Charbel Issa, P., *et al.* Optimization of in vivo confocal autofluorescence imaging of the ocular fundus in mice and its application to models of human retinal degeneration. *Invest. Ophthalmol., & Vis. Sci.* **53**, (2), 1066-1075 (2012).
50. Beynon, S. B., Walker, F. R. Microglial activation in the injured and healthy brain: what are we really talking about? Practical and theoretical issues associated with the measurement of changes in microglial morphology. *Neuroscience.* **225**, (2012), 162-171 (2012).
51. Chan, J. W. Recent advances in optic neuritis related to multiple sclerosis. *Acta Ophthalmol.* **90**, (3), 203-209 (2012).
52. Frost, S., Martins, R. N., Kanagasingam, Y. Ocular biomarkers for early detection of Alzheimer's disease. *J. Alzheimer's Dis.* **22**, (1), 1-16 (2010).
53. Guo, L., Duggan, J., Cordeiro, M. F. Alzheimer's disease and retinal neurodegeneration. *Curr. Alzheimer Res.* **7**, (1), 3-14 (2010).
54. Ikram, M. K., Cheung, C. Y., Wong, T. Y., Chen, C. P. Retinal pathology as biomarker for cognitive impairment and Alzheimer's disease. *J. Neurol. Neurosurg. Psychiatry.* **83**, (9), 917-922 (2012).
55. Kersten, H. M., Roxburgh, R. H., Danesh-Meyer, H. V. Ophthalmic manifestations of inherited neurodegenerative disorders. *Nat. Rev. Neurol.* **10**, (6), 349-362 (2014).
56. Kesler, A., Vakhapova, V., Korczyn, A. D., Naftaliev, E., Neudorfer, M. Retinal thickness in patients with mild cognitive impairment and Alzheimer's disease. *Clin. Neurol. Neurosurg.* **113**, (7), 523-526 (2011).
57. Petzold, A., *et al.* Optical coherence tomography in multiple sclerosis: a systematic review and meta-analysis. *Lancet Neurol.* **9**, (9), 921-932 (2010).
58. Satue, M., *et al.* Retinal thinning and correlation with functional disability in patients with Parkinson's disease. *Br. J. Ophthalmol.* **98**, (3), 350-355 (2014).
59. Bosco, A., Romero, C. O., Breen, K. T., Chagovetz, A. A., Steele, M. R., Ambati, B. K., Vetter, M. L. Neurodegeneration severity can be predicted from early microglia alterations monitored in vivo in a mouse model of chronic glaucoma. *Dis Model Mech.* (2015).

